Molecular Cell, Volume *47*

Supplemental Information

Structure of a Glomulin-RBX1-CUL1 Complex: Inhibition of a RING E3 Ligase through Masking of Its E2-Binding Surface

David M. Duda, Jennifer L. Olszewski, Adriana E. Tron, Michal Hammel, Lester J. Lambert, M. Brett Waddell, Tanja Mittag, James A. DeCaprio, and Brenda A. Schulman

SUPPLEMENTAL EXPERIMENTAL PROCEDURES

Constructs and protein preparation

All proteins described correspond to human sequences. The cDNA encoding Glomulin (Arai et al., 2003) was cloned in frame with GST in pGEX4T1 (GE) modified to contain a TEV proteolytic cleavage site (pGEX4T1-TEV). RBX1 (the previously-described version comprising residues 5-108)-CUL1[4HB-α/β]) (residues 411-690) used for crystallization was purified by glutathione affinity chromatography, followed by TEV proteolysis to liberate GST, and cation exchange. GLMN used for crystallization was purified by glutathione affinity chromatography, followed by TEV proteolysis to liberate GST, and anion exchange. Purified GLMN and RBX1-CUL1[4HB-α/β] were mixed 1:1 and concentrated to form a complex. The complex was purified by size exclusion chromatography in 20 mM Tris-HCl, 150 mM NaCl, 1 mM DTT, concentrated, aliquotted, flash-frozen, and stored at -80 ^{o}C. RBX1-CUL1 and RBX1-CUL1~NEDD8 refer to the "split 'n coexpress" version (Zheng et al., 2002). The versions of UBA1, UbcH5B, CDC34B (referred to in the text as CDC34), ubiquitin, APPBP1-UBA3, UBC12, NEDD8, SKP2-SKP1 (full-length), CKSHS1 (the crystallized version), p27 (the k^- version that can be phosphorylated on T187 by CDK2 (Vlach et al., 1997) also bearing the S10A mutation that restricts phosphorylation to T187 (Hao et al., 2005)), CAND1, RBX1-CUL1, RBX1-CUL1^{CTD}, RBX1-CUL1~NEDD8, and RBX1-CUL1^{CTD}~NEDD8 used in biochemical and biophysical experiments were described previously (Duda et al., 2008; Huang et al., 2009; Huang et al., 2008; Jubelin et al., 2010; Schulman et al., 2000; Siergiejuk et al., 2009; Walden et al., 2003; Zheng et al., 2002). Kinase active CyclinA (residues 174-432)-CDK2 was prepared by separate glutathione affinity purification of GST-CyclinA$^{174-432}$ and GST-CDK2 (coexpressed bicistronically with GST-Cak1p from a home-made modified pGEX vector), mixing the two GST-fusion proteins and co-cleaving with TEV protease, followed by purification of the complex by cation exchange and gel filtration chromatography. FBW7-SKP1 (full-length proteins in the complex) was prepared by coexpression of GST-FBW7 and SKP1 in insect cells, followed by glutathione affinity chromatography, cleavage with TEV protease to remove GST, and purification by anion exchange and gel filtration chromatography. For biochemical and Biacore experiments, the isolated RING domains from RBX1 (residues 36-108, referred to as RBX1^{RING}), RBX2 (residues 44-113, referred to as RBX2^{RING}), and APC11 (residues 17-85, referred to as APC11^{RING}) were initially purified as GST, His-MBP, and GST fusions, respectively, and purified by gel filtration chromatography after treatment with TEV protease to remove the tags.

For FRET-based binding studies GLMN-YFP, CFP-RBX1^{RING}, CFP-RBX1 (residues 5-108), CDC34B-YFP and CDC34B (residues 153-C)-YFP (referred to hereafter as CDC34^{TAIL}) were expressed as GST-fusions from pGEX4T1-TEV. For CDC34 binding studies, a fluorescent RBX1-CUL1 was generated by modifying the previously published "split 'n coexpress" system (Zheng et al., 2002), with the C-terminus of CUL1^{CTD} fused via a short linker to CFP, and RBX1 expressed either as wild-type protein or as a version with the RING domain deleted (RBX1$^{\Delta RING}$). Following glutathione affinity chromatrography and treatment with TEV or thrombin protease to liberate GST, the FP-fusion proteins were purified by ion exchange chromatography. For the GLMN binding studies, CFP-RBX1^{RING} and CFP-RBX1-CUL1^{CTD} (both unmodified and quantitatively neddylated as described (Duda et al., 2008)) were purified by gel filtration into a final buffer 25 mM Tris-HCl (pH 7.6), 150 mM NaCl, 1 mM DTT. RBX1-CUL1^{NTD}-CUL^{CTD}-CFP, RBX1$^{\Delta RING}$-CUL1^{NTD}-CUL^{CTD}-CFP, CDC34-YFP, and CDC34^{TAIL}-YFP were purified by gel filtration into a final buffer 25 mM Tris-HCl (pH 7.6), 100 mM NaCl, 1 mM DTT. Peak fractions were pooled, aliquotted and flash-frozen prior to use.

RBX1^{RING} used for NMR experiments was expressed as an N-terminal His-SUMO fusion protein where TEV cleavage yields an N-terminal GSGG sequence fused to a version of RBX1 spanning residues 36-108. Expression was in BL21(DE3) cells in either ^{15}N or $^{15}N/^{13}C$ enriched minimal media. Induction yielded the protein in the form of insoluble inclusion bodies. Collected cells were lysed by sonication, subjected to centrifugation and the soluble lysate discarded. The insoluble pellet was homogenized multiple times in 50 mM Tris pH 8.4, 6 M guanidine. After clarification by centrifugation, the lysate containing unfolded protein was immobilized on nickel sepharose (GE-Healthcare), and the column washed with a buffer of 50 mM Tris pH 8.4, 0.2 M NaCl, 10 μM $ZnSO_4$, 4.0 M urea, 30 mM imidazole, and 20% glycerol. The protein was eluted in 50 mM Tris pH 8.4, 0.2 M NaCl, 10 μM $ZnSO_4$, 1.0 M urea, 300 mM imidazole and 20% glycerol. The protein solution was adjusted to 10 mM β-mercaptoethanol and treated with TEV protease for 12 hours at 4°C. After concentration, the cleaved protein mixture was purified to homogeneity by size-exclusion chromatography (HiLoad 16/60 Sephacryl 75) in a column buffer of 50 mM Tris pH 8.2, 0.2 M NaCl, 1 M urea, 10 mM β-mercaptoethanol, and 10 μM $ZnSO_4$. To obtain purified isotopically enriched RBX1^{RING}, pooled peak fractions were concentrated using stirred-cell ultrafiltration (Millipore) and dialyzed against a buffer of 1X PBS pH 7.0, 10 mM DTT, 10 μM $ZnSO_4$ that displayed modest precipitation from the DTT/$ZnSO_4$ mixture.

Protein concentrations were determined based on A280 absorbance with a Nanodrop spectrophotometer.

Crystal structure determination

In a comprehensive effort to crystallize GLMN (or GLMN's C-terminal domain) bound to any form of RBX1, we obtained crystals of GLMN complexes with RBX1-CUL1(split 'n coexpress)-CAND1, with RBX1-CUL1^{CTD}~NEDD8 and with RBX1-CUL1^{CTD}. Although the majority of the crystals were radiation sensitive and/or diffracted poorly, we were able to obtain an initial electron density map from crystals of SeMet-labeled GLMN complexed with RBX1-CUL1^{CTD} by MR-SAD after merging 9 different SAD datasets (including inverse beam data) to obtain nearly complete data at 3.5 Å resolution. PHENIX AUTOSOL (Adams et al., 2010), combining a partial MR solution (trimmed from 1LDJ.PDB to contain CUL1 residues 420-690 and RBX1 residues 19-35) with SAD data from crystals where GLMN was SeMet labeled, identified 22 out of 28 GLMN Se sites in the asymmetric unit, and an additional six sites corresponding to the six total zinc ions present in the RING domains of the two molecules of RBX1. Initial maps showed continuous density over CUL1's 4HB and α/β domains as well as RBX1's N-terminal β-strand. Electron density for the RING domains of the two RBX1 molecules was visible but fragmented. Strong anomalous density for all three zinc ions per RBX1 RING, not only from the SeMet data but also obtained in a separate dataset collected using a wavelength of 1.28 Å, allowed unambiguous placement of the RING domains. Additionally, there was clear density for 22 α-helices corresponding to GLMN. However, density for connections between the helices was very sparse, precluding determining the directions of the helices or matching sequence even with the known selenium positions. To solve this problem, we applied the method of selenomethionine scanning mutagenesis (Huang et al., 2004). 28 individual site-specific mutations were made to incorporate additional selenomethionine residues, one at a time, within GLMN (Fig. S1). Of these, 19 mutants yielded proteins/crystals/diffraction/clear additional anomalous density. These were: L6M, L31M, L45M, C72M, L88M, L103M, L124M, V188M, F226M, L282M, L343M, L390M, L403M, L446M, L465M, L498M, A530M, L567M, and A573M. Anomalous difference maps

allowed for the unequivocal placement of each individually added selenomethionine in the structure. CUL1's helix 29 and WHB subdomain, which correspond to regions we previously found undergo rotations in CRLs, were not observed in the electron density maps, and thus were deleted in the construct used for final structure refinement, for which we obtained data to 3 Å resolution. In the final structure, electron density remained low quality for portions of GLMN helices 1-7. There is some uncertainty for side-chains in this region, which were placed based on SeMet locations and reasonable density for the backbone and many side-chains for one copy of the complex in the asymmetric unit. This region is distal from the RBX1-binding site, which involves helices 18-22. Several loops in GLMN, RBX1, and CUL1[4HB-α/β] not visible in the electron density were not modeled in the final refined structure.

Crystals of GLMN-RBX1-CUL1[4HB-α/β] were grown by the hanging drop vapor diffusion method with protein mixed 1:1 with well buffer consisting of 18-21% PEG 3350, 0.2 M ammonium citrate pH 7.0, 5% ethylene glycol and 5 mM DTT. Crystals were flash-frozen in 21% PEG3350, 250 mM ammonium citrate pH 7.0, 20% ethylene glycol, 12% xylitol. Crystals of GLMN-RBX1-CUL1[4HB-α/β] and GLMN-RBX1-CUL1^{CTD} where GLMN was selenomethionine labeled were prepared under similar conditions. All data were processed and scaled with HKL2000 (Otwinowski and Minor, 1997). The crystals form in the spacegroup $P2_1$, with two complexes per asymmetric unit. Data were collected at the 8.2.1 and 8.2.2 beamlines at ALS, and at ID-24 (NECAT) beamline at APS. The structure was built using Coot (Emsley and Cowtan, 2004), and refined using a combination of CNS (Brünger et al., 1998) and PHENIX (Adams et al., 2010).

SAXS data collection and evaluation

SAXS data were collected at the ALS beamline 12.3.1 (SIBYLS) LBNL Berkeley, California (Hura et al., 2009). Data were collected using a wavelength λ=1.0 Å and with the sample-to-detector distances set to 1.5 m resulting in scattering vectors, q, ranging from 0.01 Å-1 to 0.33 Å-1. The scattering vector is defined as $q = 4\pi \sin\theta/\lambda$, where 2θ is the scattering angle. All experiments were performed at 20°C and data were processed as described (Hura et al., 2009). The program GNOM (Svergun, 1992) was used to compute the pair-distance distribution functions, P(r). The overall shapes for both unneddylated complexes (GLMN-RBX1-CUL1 and GLMN-RBX1-CUL1^{CTD}) were restored from the experimental data using the program GASBOR with P_1 symmetry operator (Svergun et al., 2001). In our rigid body modeling strategy BILBOMD, molecular dynamics (MD) simulations were used to explore conformational space adopted by GLMN, GLMN-RBX1, GLMN-RBX1-CUL1^{CTD}~NEDD8 and GLMN-RBX1-CUL1~NEDD8 complexes (Pelikan et al., 2009). For each registered conformation, the theoretical SAXS profile and the corresponding fit to the experimental data were calculated using the program FoXS (Schneidman-Duhovny et al., 2010). A Minimal Ensemble Search (MES) was used to select two conformers from a pool of all generated conformers that achieved the best fit to the experimental curve (Pelikan et al., 2009). Comparison of the structural properties of the selected conformers allowed us to distinguish the degree of flexibility and heterogeneity of the experimental system.

Enzyme assays

For all assays, proteins were desalted into 20 mM Tris pH 7.6, 20 mM NaCl aliqotted and stored. Polyubiquitination assays of phospho-p27-CyclinA-CDK2 and phospho-cyclinE peptide were adapted from those previously described (Duda et al., 2008; Jubelin et al., 2010). In these assays, wild-type or mutant GLMN was incubated with NEDD8-modified RBX1-CUL1 for 10 minutes prior to adding other SCF components and initiating the reactions. Briefly, for the substrate polyubiquitination assays, the

concentration of the neddylated SCF complex was 200 nM, and for all figures except 5E, the concentration of CDC34 was 500 nM. For Fig. 2D, the concentration of GLMN ranged from 50 nM to 1 μM. For Fig. 5E, the concentration of GLMN was either 200 nM or 600 nM (1x or 3x relative to SCF). For all other polyubiquitination assays, the concentration of wild-type or mutant GLMN was 600 nM. For Fig. 5E, the concentration of CDC34 ranges from 500 nM to 6 μM. We used low salt to minimize any effects that salt may have on CDC34 tail binding to CUL1 (Kleiger et al., 2009), with a reaction buffer of 10 mM $MgCl_2$, 5 mM ATP, 30 mM Tris pH 7.6, and 20 mM NaCl, with 250 nM UBA1, and 1 mg/ml BSA. Reactions contained 50 μM Ub, except the experiment in Fig. 5E, which contained 100 μM Ub. Reactions were initiated by addition of UBA1, and performed at room temperature for the indicated times. For the SCF^{FBW7} polyubiquitination assays, 5 μM of a biotinylated CyclinE phosphopeptide was used as the substrate (Jubelin et al., 2010), and reactions were quenched in 2X SDS-PAGE sample buffer containing 50 mM DTT. Ubiquitinated substrate was detected by western blot using an anti-biotin Ab (Rockland, 100-4198). For the $SCF^{SKP2\text{-}CKSHS1}$ polyubiquitination assays, p27 (5 μM) was phosphorylated by incubation with 5 μM CyclinA-CDK2 in 40 mM Tris pH 7.6, 10 mM $MgCl_2$, 1 mM ATP, 1 mM DTT at 30°C for 30 minutes. This was diluted into the reaction mix to a final concentration of 0.2 μM phospho-p27-CyclinA-CDK2. $SCF^{SKP2\text{-}CKSHS1}$ polyubiquitination assays also contained 250 nM UbcH5B. These reactions were quenched in 2X SDS-PAGE sample buffer containing 50 mM DTT and 8 M urea, and were incubated at 100 °C for 1 minute prior to loading on gels, with ubiquitinated phospho-p27 detected using the sc-16324 antibody from Santa Cruz. For experiments examining relief of GLMN inhibition by addition of the isolated RBX1 RING domain, the concentration of $RBX1^{RING}$ was 200 nM (1x) or 600 (3x) nM in Fig. 2E and Fig. 2F, and 600 nM in Fig. 4E. Here, $RBX1^{RING}$ (and mutants) and GLMN were mixed for 10 minutes on ice, prior to mixing with NEDD8-modified RBX1-CUL1 for 10 minutes, followed by adding other assay components.

For assays examining substrate-independent CRL-stimulated di-Ub chain formation by the E2, CDC34, K0 ubiquitin (all lysines mutated to arginines) with an N-terminal poly-glycine sequence was purified to facilitate sortase-mediated transpeptidation (Antos et al., 2009; Spirig et al., 2011) to incorporate a fluorescein-conjugated peptide (Fluorescein-$(PEG)_5$-LPRTGG-COOH) onto the Ub K0 N-terminus. 10 μM CDC34 was charged in the presence of 20 μM fluorescein-ubiquitin K0 and 150 nM Uba1 in 25mM Tris-HCL (pH 7.6), 2.5 mM MgCl2, 2.5 mM ATP for 25 minutes at room temperature. The charging reaction was quenched by diluting 5-fold into buffer containing 25 mM Tris-HCl (pH 7.6), 50 mM EDTA for 5 minutes at room temperature. This reaction was diluted 10-fold into chase mixes at room temperature, containing 25 mM Tris (pH 7.6), 100 mM NaCl, 500 μM Ub (SIGMA), 0.25 mg/ml BSA, 50 mM EDTA, and where indicated 500 nM RBX1-CUL1~NEDD8 and 2 μM GLMN. Samples were removed from the reactions at the indicated time points, and reactions were stopped by the addition of nonreducing SDS-PAGE sample buffer. Proteins were resolved by SDS-PAGE and visualized on a STORM Phosphorimager at 450 nm.

Binding assays

To examine co-association during gel filtration chromatography, proteins were mixed at an equimolar concentration of 9 μM for at least 10 minutes on ice. 200 μl of each mix was loaded onto an SD200 10/300 column (GE), with a running buffer of 25 mM Tris pH 7.6, 150 mM NaCl, 1 mM DTT. Fractions from gel filtration chromatography were analyzed by SDS-PAGE, with proteins detected by staining with Sypro Ruby (Bio-Rad).

For FRET experiments, donor and acceptor containing proteins were mixed for 5 minutes in a buffer containing 25 mM Tris-HCl (pH 7.6), 50 mM NaCl at 22 °C before all measurements. Fluorescence measurements were carried out on a FluoroMax-4 spectrofluorometer (HORIBA Scientific). For each point in the titrations, a separate sample was made so as not to have artifacts from photobleaching.

In the FRET experiments in Fig. 2G, the concentrations of CFP-RBX1^{RING}, CFP-RBX1-CUL1^{CTD} and CFP-RBX1-NEDD8~CUL1^{CTD} were held constant at 5 nM. GLMN-YFP was titrated from 0-300 nM using the following concentrations: 0, 2.5, 5, 10, 20, 30, 40, 60, 80, 100, 150, 200, and 300 nM. The excitation wavelength was 420 nm, and emission was scanned from 440-600 nm.

In the FRET experiments in Fig. S3, RBX1-CUL1-CFP or RBX1$^{\Delta RING}$-CUL1-CFP were held at a constant concentration of 5 nM, titrating CDC34-YFP or CDC34^{TAIL}-YFP from 0-160 nM using the following concentrations: 0, 2.5, 5, 10, 20, 40, 80, and 160 nM. The excitation wavelength was 430 nm, and emission was scanned from 440-600 nm.

The FRET efficiency (E) was determined by taking the maximum fluorescence intensity for the donor (CFP-conjugate) at 475 nm in the presence (F_{DA}) and absence (F_D) of acceptor (GLMN- or CDC34- or CDC34^{TAIL}-YFP fusion protein) and solving for E=1-(F_{DA}/F_D). Kd was estimated by fitting of the titration curves to a hyperbolic equation assuming a single-site binding model using the program GraFit (Erithacus).

For Biacore analyses, GLMN was minimally biotinylated by reaction with EZ-Link Sulfo-NHS-LC-LC-Biotin (Thermo Scientific). The biotin reagent was added to the protein at a 0.5:1 molar ratio, and the reaction was incubated on ice for 3-6 hours. Unconjugated biotin was removed by processing the samples through two Zeba Spin Desalting Columns (Thermo Scientific) that had been equilibrated with storage buffer (20 mM Tris (pH 7.6), 150 mM NaCl, 5 mM DTT, and 5% glycerol). Bovine serum albumin (BSA) was added to the reaction at a final concentration of 0.1 mg/mL immediately prior to processing through the spin columns to improve recovery (Papalia and Myszka, 2010).

Kinetic binding studies were performed at 25°C using a Biacore 3000 SPR instrument (GE Healthcare). Streptavidin (Thermo Scientific) was covalently attached to a carboxymethyl dextran-coated gold surface (CM-4 Chip; GE Healthcare). The carboxymethyl groups of dextran were activated with *N*-ethyl-*N*′-(3-dimethylaminopropyl) carbodiimide (EDC) and *N*-hydroxysuccinimide (NHS), and streptavidin was immobilized at pH 4.5 in 10 mM sodium acetate to levels of ~780-950 RU/flowcell. Any remaining reactive sites were blocked by reaction with ethanolamine. Biotinylated Glomulin was injected over the streptavidin surfaces until ~480-530 RU had been captured.

The kinetics of association and dissociation were monitored at a flow rate of 50 μl/min. The RINGs were prepared as 3-fold dilution series in running buffer (20 mM Tris pH 7.6, 150 mM NaCl, 1 mM TCEP, 5% glycerol, and 0.005% Tween20) ranging from 6.3 to 510 nM for wild-type and the Arg91Ala mutant version of the isolated RBX1 RING domain and wild-type GLMN or GLMN mutants, and from 63 nM to 5.1 μM for experiments with wild-type GLMN and the Glu55Ala, Gln57Ala, Gln57Ala/Arg91Ala mutants of the RBX1 RING domain, RBX2^{RING} and APC11^{RING}. The RING proteins dissociated completely from the chip surface, eliminating the need for a regeneration step. Triplicate injections were made at each concentration, and the data were processed, double-referenced and analyzed with the software package Scrubber2 (version 2.0b, BioLogic Software) (Myszka, 1999). The kinetic rate constants and/or equilibrium

dissociation constants were determined by fitting the data to a 1:1 (Langmuir) interaction model.

Cell transfection, Immunoprecipitation and Immunoblotting

Plasmids expressing HA-tagged wild-type (Tron et al., 2012) and mutant versions of GLMN or empty vector (EV) were transfected into HEK293T cells using Lipofectamine2000 (Invitrogen), according to the manufacturer's instructions. Cells were lysed in NTEN buffer [20 mM Tris (pH 8.0), 100 mM NaCl, 1 mM EDTA and 0.5% NP-40] supplemented with protease inhibitors (Cocktail Set I; Calbiochem) 48 hours after transfection. Protein concentrations of the lysates were measured using Bradford Protein Assay reagent (Bio-Rad) on a DU 640 spectrophotometer (Beckman Coulter). The lysates were then resolved by SDS-PAGE and immunoblotted with antibodies against RBX1 (Ab1; LabVision); CUL1 (C-terminal domain detection: 32-2400; Invitrogen; N-terminal domain detection: H213; Santa Cruz); HA (HA-11; Covance); and Vinculin (V9131; Sigma). For immunoprecipitations, 1.5 mg of lysates were incubated with agarose conjugated HA antibody (HA-F7; Santa Cruz) for 4h at 4ºC. Immuno-complexes were washed five times with NTEN buffer before being resolved by SDS-PAGE and immunoblotted with the indicated antibodies.

To quantify the relative amounts of GLMN, RBX1, and CUL1, we ran western blots of lysate loaded side-by-side with standards of known, increasing amounts of these purified proteins. We quantified the bands using a Syngene imaging system, and compared the intensity of the band from the lysate with the calibration curves generated from the standards. Based on our measurement of 0.216 ng of total protein/cell, and the number of picomoles of GLMN, RBX1, and CUL1 per 25 or 50 μg lysate protein, we calculate 0.001 femtomoles of GLMN, 0.077 femtomoles of RBX1, and 0.005 femtomoles of CUL1 per cell. We next compared this to an IP with GLMN. Bearing in mind the limitations of determining complex concentrations by IP, we estimate that GLMN binds 7.3% of the total pool of RBX1 in the cell and 0.16% of the total pool of intracellular CUL1.

NMR spectroscopy

Samples of RBX1 (0.212 mM), CDC34 (1.0 mM) and GLMN (0.38 mM) were dialyzed for 2 days at 4°C against an identical buffer of 1X PBS pH 7.0, 10 mM DTT and 10 μM $ZnSO_4$ (that displayed modest precipitation from the DTT/$ZnSO_4$ mixture) using a D-tube Midi microdialyzer MWCO 3.5 kDa (Novagen, USA). D_2O/DSS were added to 10% and 0.33 mM. For NMR experiments, the inhibitor GLMN or the CDC34 protein were mixed separately in an Eppendorf tube and the samples transferred to an NMR tube at a normalized uniform volume. All NMR experiments were recorded at 298 K using a Bruker AVANCE 600 MHz NMR spectrometer equipped with a cryoprobe. Two dimensional [^{1}H,^{15}N] TROSY spectra with 2048 X 180 complex points, 16 or 32 scans and Watergate water suppression were collected for free ^{15}N RBX1^{RING} and successive additions of GLMN to 0.5, 1 and 1.5 equivalents or for additions of CDC34 to 0.5, 1, 3.6 and 5.5 equivalents. For the binding competition assay, 1 and 2 molar equivalents of GLMN were added to the final ^{15}N RBX1:CDC34 complex. The NMR data were processed using NMRPipe (Delaglio et al., 1995); data analysis employed Sparky (Goddard and Kneller). Assignments of the spectrum of RBX1 closely matched those reported for a related construct during manuscript revision (Spratt et al., 2012), with confirmation of Cα chemical shifts provided by analysis of a 3D HNCA experiment. Similarly, RBX1^{RING} resonances we found to undergo csp upon binding to CDC34 also match those reported during manuscript revision to undergo csp upon binding to CDC34A (Spratt et al., 2012).

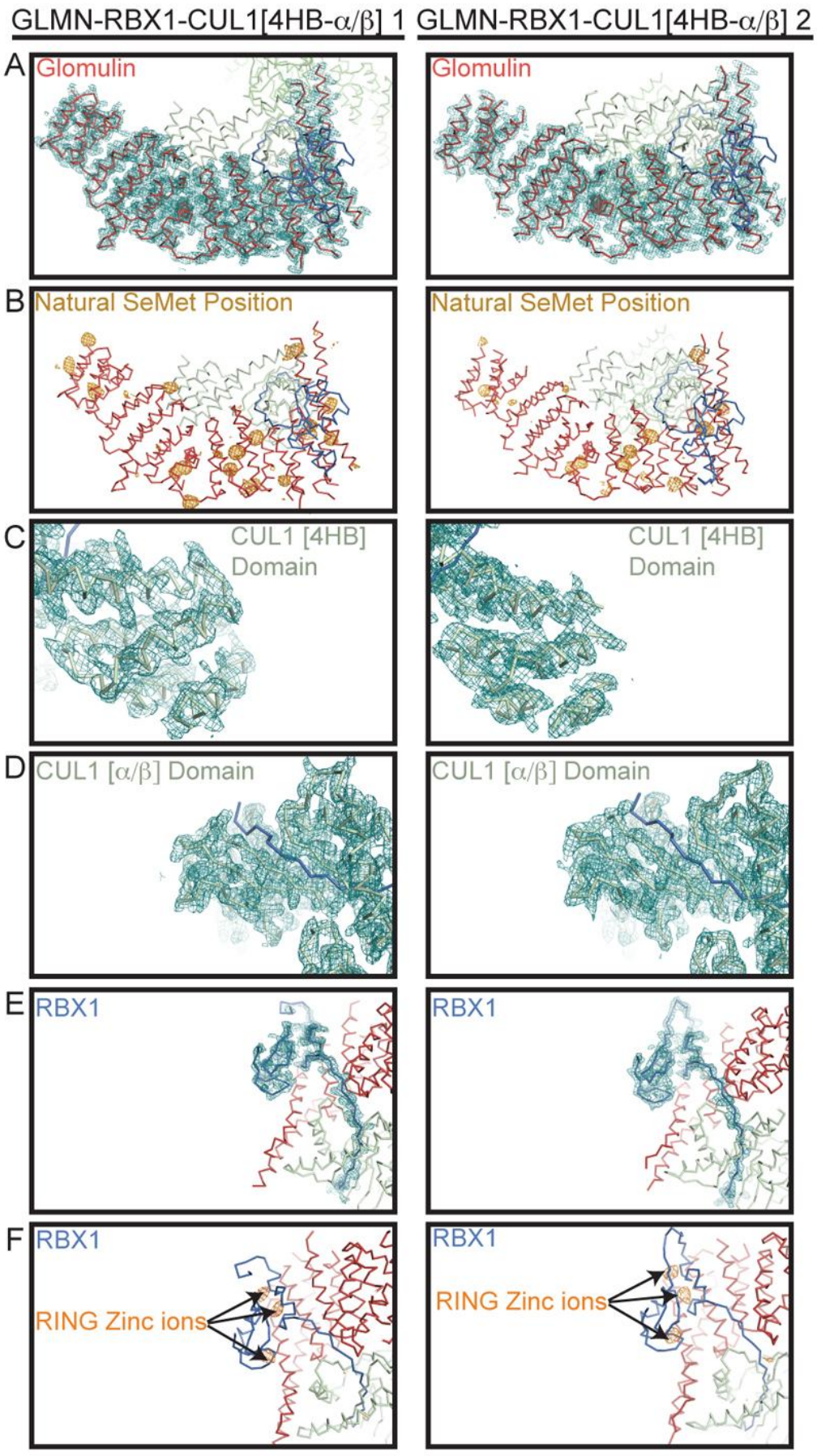
GLMN-RBX1-CUL1[4HB-α/β] 1
GLMN-RBX1-CUL1[4HB-α/β] 2
A
Glomulin
Glomulin
B
Natural SeMet Position
Natural SeMet Position
C
CUL1 [4HB] Domain
CUL1 [4HB] Domain
D
CUL1 [α/β] Domain
CUL1 [α/β] Domain
E
RBX1
RBX1
F
RBX1
RING Zinc ions
RBX1
RING Zinc ions

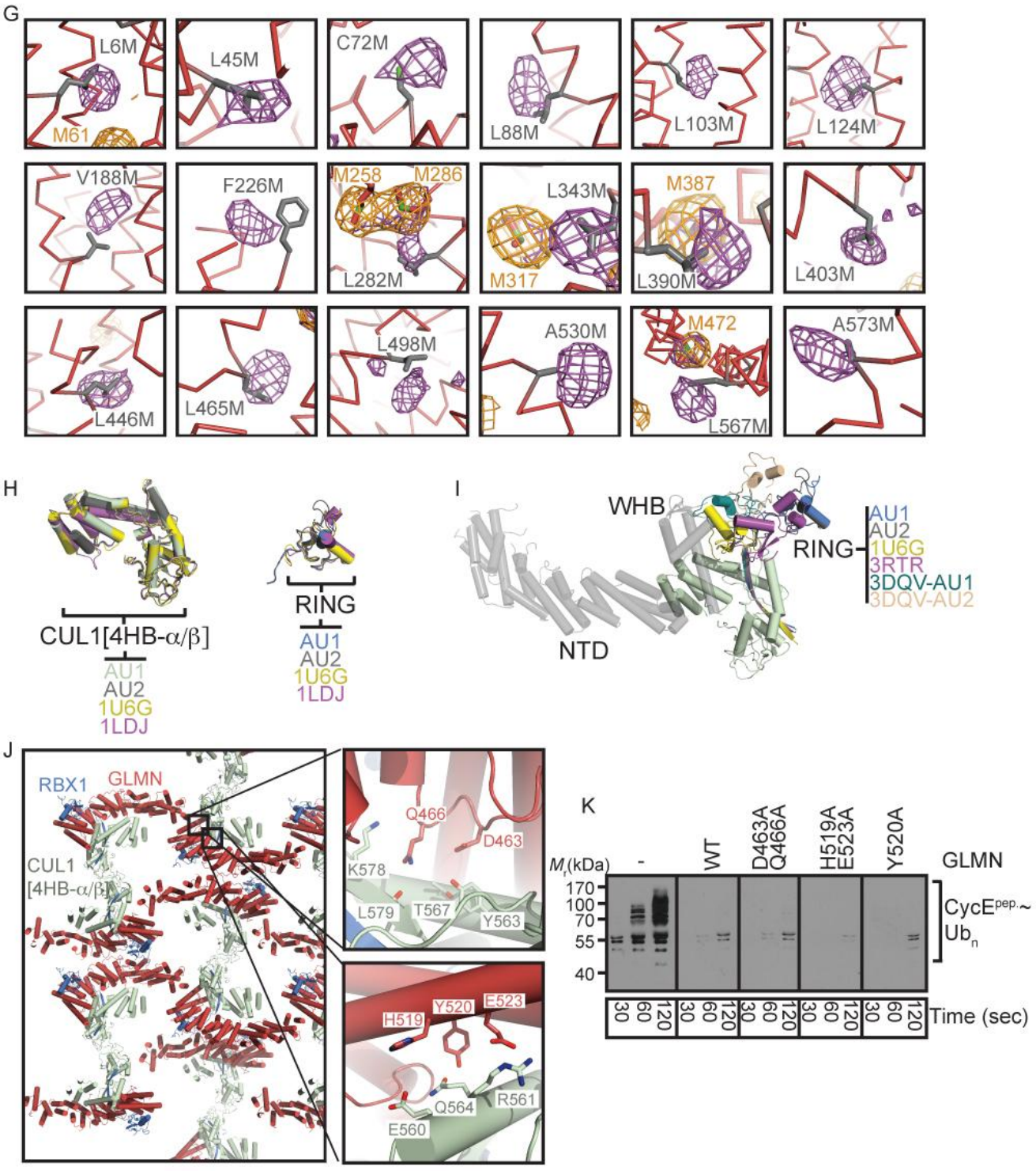

Figure S1. Crystal structure of GLMN-RBX1-CUL1[4HB-α/β]

A. Final $2F_o$-F_c electron density over both copies of GLMN in the asymmetric unit, contoured at 1σ.

B. Anomalous difference density contoured at 3σ from data collected using wavelength of 0.979 Å observed for selenomethionine-labeled wild-type GLMN is shown in orange for both copies in the asymmetric unit.

C. Final $2F_o$-F_c electron density over both copies of the CUL1 4HB subdomain in the asymmetric unit, contoured at 1σ.

D. Final $2F_o$-F_c electron density contoured at 1σ over both copies of the CUL1 α/β-subdomain in the asymmetric unit.

E. Final $2F_o$-F_c electron density contoured at 1σ over both copies of RBX1 in the asymmetric unit.

F. Anomalous difference density contoured at 3σ from data collected at the zinc edge of 1.28 Å displayed over the zinc atoms from RBX1 for both copies in the asymmetric unit.

G. Close-up views of anomalous difference density maps contoured at 3σ in purple for one complex in the asymmetric unit, from data collected using wavelength of 0.979 Å for crystals from each of 18 of the 19 individual selenomethionine mutant versions of GLMN used to guide structure determination. Nearby density for native selenomethionines in some of the mutants is shown in orange. For ease of display, the anomalous difference density map for the L31M mutant is not shown.

H. Superposition of individual domains onto prior CUL1-RBX1 structures (Goldenberg et al., 2004; Zheng et al., 2002), for both copies of CUL1[4HB-α/β] (left) or RBX1 RING (right) from the asymmetric unit. Structures are colored according to the labels for PDB codes, with AU1 and AU2 referring to the two complexes in the asymmetric unit.

I. Superposition of the CUL1[4HB-α/β] portion of the GLMN-RBX1-CUL1[4HB-α/β] complex onto the corresponding regions of RBX1-CUL1-CAND1 (1U6G.pdb, representing most commonly observed RBX1 RING orientation) (Goldenberg et al., 2004), RBX1-$CUL1^{CTD}$ (RING domain in conformation poised for neddylation, 3RTR.pdb) (Calabrese et al., 2011), RBX1~$CUL5^{CTD}$~NEDD8 (3DQV.pdb, demonstrating RING domain flexibility) (Duda et al., 2008) showing all the different relative orientations for the RBX1 RING domain observed in different structures. For reference, the CUL1 N-terminal domain and WHB subdomain from 1U6G.pdb are shown in grey. Structures are colored according to the labels for PDB codes, with AU1 and AU2 referring to the two complexes in the asymmetric unit.

J. Arrangement of GLMN (red)-RBX1 (blue)-CUL1[4HB-α/β] (light green) complexes in the crystal. Crystal packing contacts between GLMN and CUL1 are highlighted in panels on the right.

K. Anti-biotin western blots showing time-courses of SCF^{FBW7}-mediated polyubiquitination of a biotinylated CyclinE phosphopeptide, in the presence of 3x GLMN:SCF for either wild-type or the indicated versions of GLMN mutated for residues making crystal contacts with CUL1.

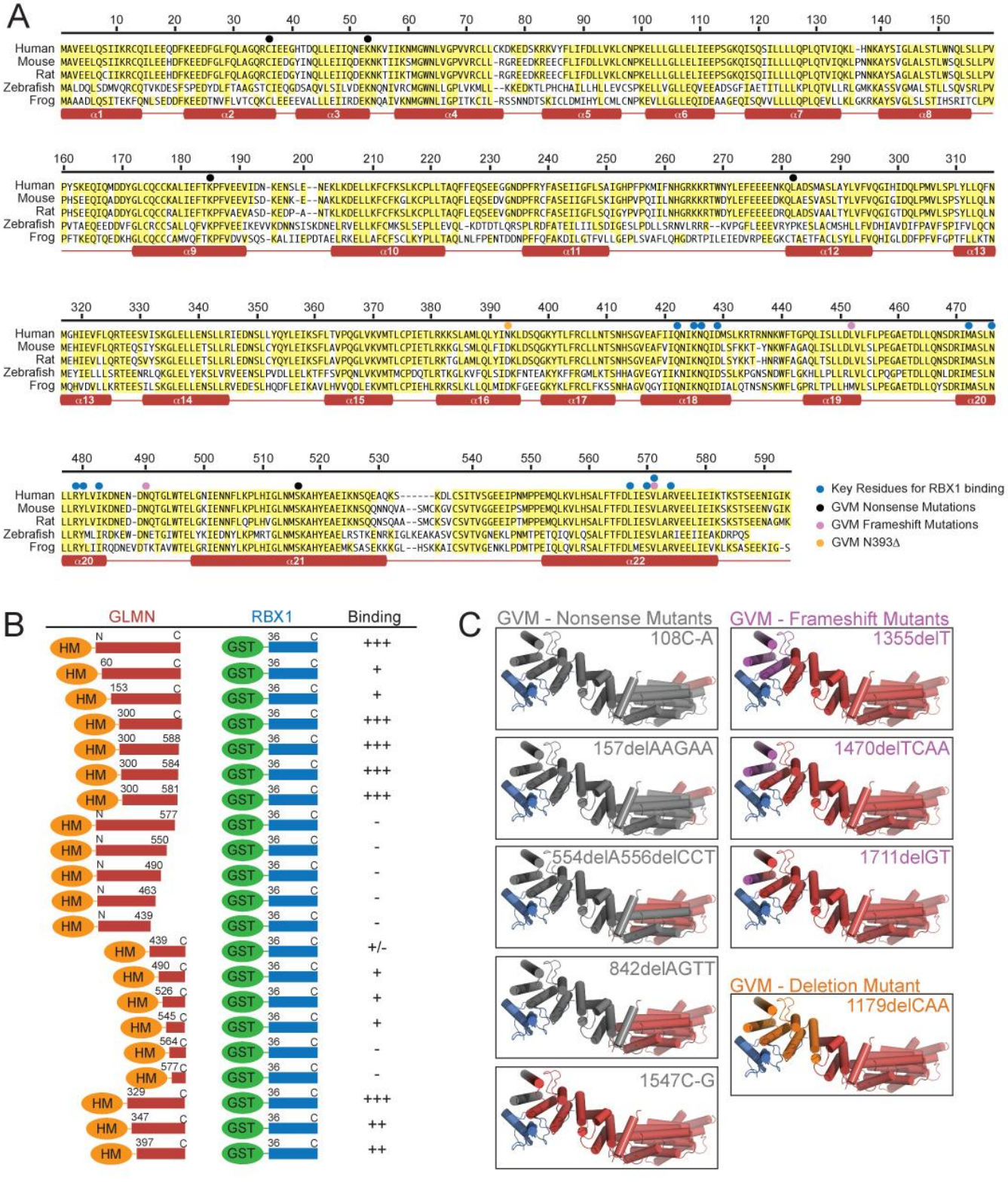

Figure S2. Structural features of GLMN

A. Alignment of human GLMN sequence with that from mouse (*Mus musculus*), rat (*Rattus Norvegicus*), zebrafish (*Danio rerio*), and frog (*Xenopus laevis*), with identity to the

human sequence highlighted in yellow. Above the sequence, key residues for RBX1 binding are indicated with blue dots, and locations of Glomuvenous Malformation disease-associated nonsense, frameshift, and deletion mutations are indicated with black, pink, and yellow dots, respectively. Secondary structures for human GLMN are denoted below.

B. Summary of domain mapping of GLMN interactions with RBX1 RING domain, performed by copulldown of the indicated His-MBP-fusions (HM) of GLMN fragments coexpressed with GST-RBX1^{RING}.

C. Locations of GVM disease-associated mutations mapped onto the RBX1-GLMN portion of the structure. Portions of GLMN deleted or mutated due to nonsense, frameshift, or deletion mutations are shown in grey, purple, or orange, respectively, with the portion of GLMN not affected by mutations shown in red. Mutations are indicated by the position in the GLMN ORF sequence that is the site of the mutation. Del refers to the bases deleted at that site. C-G refers to a C-to-G mutation.

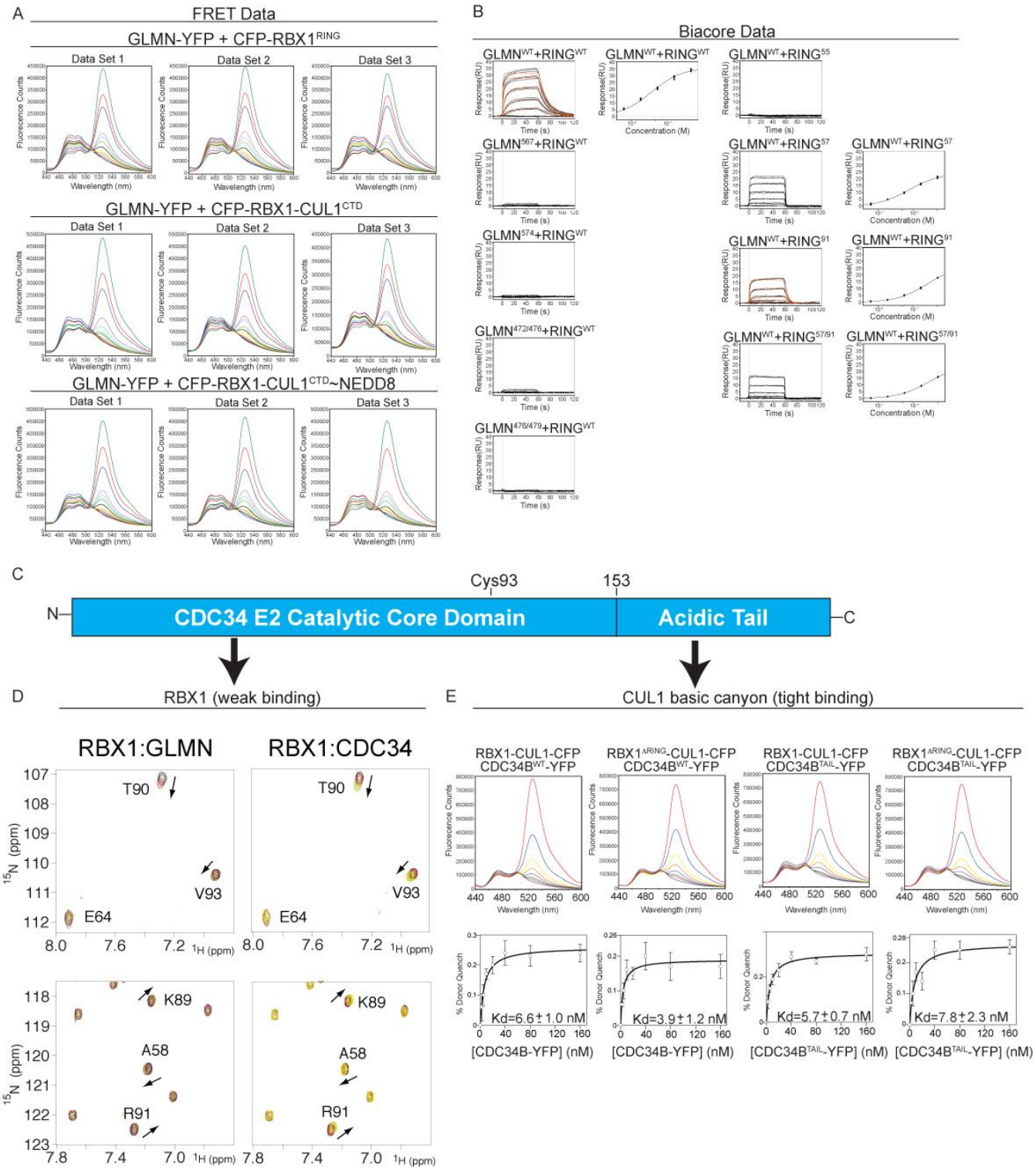

Figure S3. Data for RBX1 binding to GLMN or CDC34

A. Primary data for binding studies performed by FRET, with 5 nM CFP-RBX1^{RING}, CFP-RBX1-CUL1^{CTD}, or CFP-RBX1-CUL1^{CTD}~NEDD8 and 0, 2.5, 5, 10, 20, 30, 40, 60, 80, 100, 150, 200, and 300 nM GLMN-YFP, using an excitation wavelength of 420 nm.

B. Representative sensorgrams with curve fits for kinetic binding analyses in orange, and where applicable equilibrium binding curves from Surface Plasmon Resonance interaction assays, performed using Biacore for wild-type or the indicated mutants of GLMN and wild-type $RBX1^{RING}$ (left) or wild-type GLMN and the indicated mutants of $RBX1^{RING}$ (right).

C. Schematic view of CDC34 structure based on linear sequence. CDC34 consists of an N-terminal E2 catalytic core domain that binds RBX1's RING domain (Spratt et al., 2012), and a C-terminal acidic tail that binds with high affinity to a basic canyon in CUL1 (Kleiger et al., 2009).

D. Sections of [$^{1}H^{N}$, ^{15}N] TROSY spectra of ^{15}N $RBX1^{RING}$ alone (black), and for successive additions of $GLMN^{300-594}$ (left) at 0.5 (red), 1 (green) and 1.5 equivalents (gold), or for additions of CDC34 (right) at 1.0 (red), 3.6 (green) and 5.5 equivalents (gold). $GLMN^{300-594}$ binding leads to successive chemical shift perturbations and to extensive line broadening due to the high affinity and anisotropy of the complex. Weak binding of CDC34 (estimated K_D > 1mM (Spratt et al., 2012)) results in chemical shift perturbations with little line broadening even at 5.5-fold molar excess.

E. Top - Primary data for binding studies performed by FRET, with 5 nM RBX1 or $RBX1^{\Delta RING}$ complexed with split 'n coexpress CUL1-CFP and 0, 2.5, 5, 10, 20, 40, 80, and 160 nM CDC34-YFP or $CDC34^{TAIL}$-YFP, using an excitation wavelength of 430 nm. Bottom – Quantification of dissociation constant (mean ± SD) from FRET-based binding assay. Error bars represent standard error from 3 independent experiments.

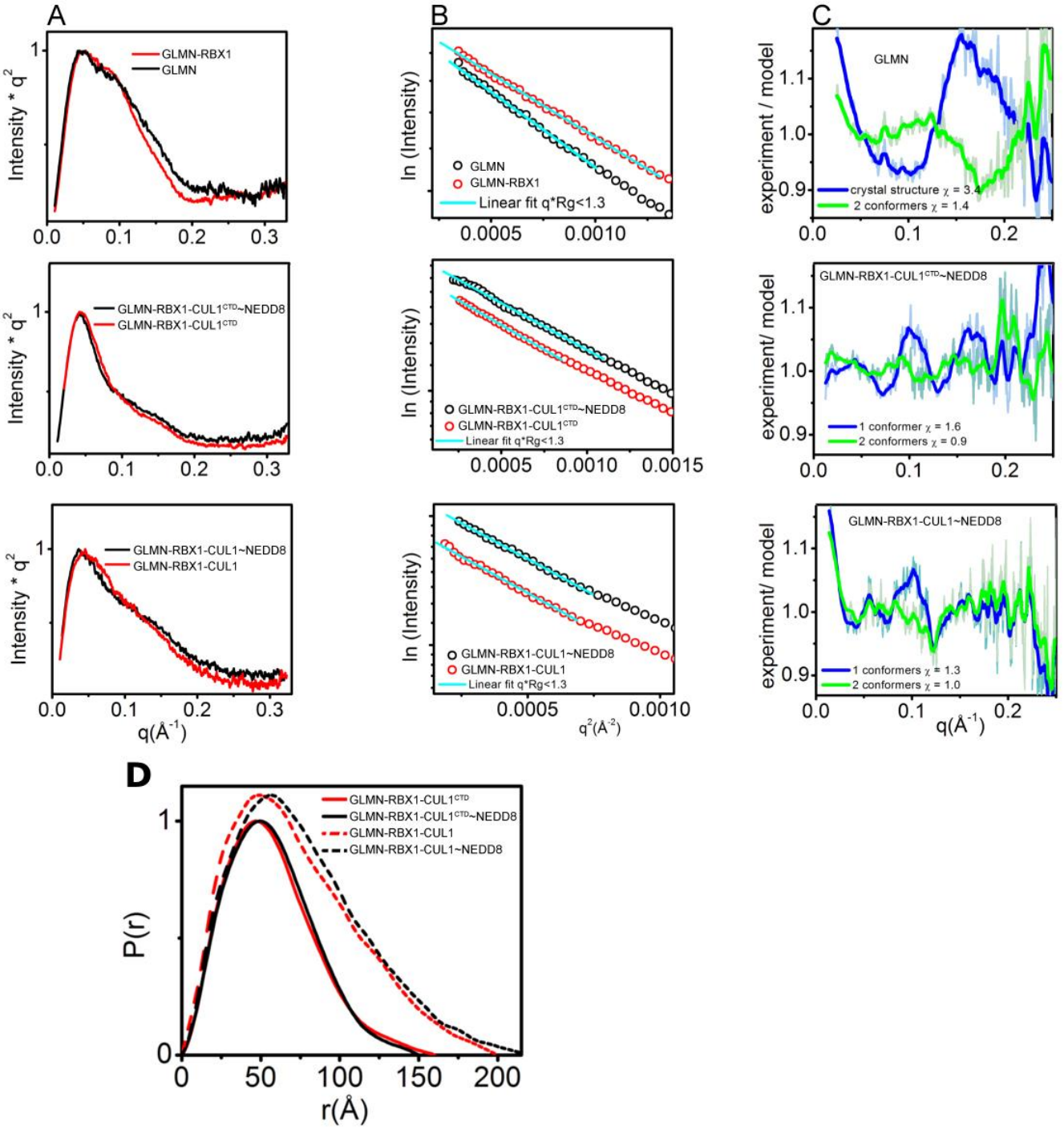

Figure S4. Small Angle X-ray Scattering (SAXS) analyses

A. Experimental SAXS curves shown as a Kratky plots indicate higher flexibility for GLMN alone as compared to in the GLMN-RBX1, GLMN-RBX1-CUL1^{CTD}, GLMN-RBX1-CUL1^{CTD}~NEDD8, GLMN-RBX1-CUL1, and GLMN-RBX1-CUL1~NEDD8 complexes.

B. Giunier plots with Giunier regions. A linear dependence of ln(I(q)) vs. q^2 indicates the aggregation free sample. Radius of gyration (Rg) values as obtained from Giunier plots: GLMN Rg=45.0±0.4; GLMN-RBX1 Rg=39.1.0±0.3; GLMN-RBX1-CUL1^{CTD} Rg=

44.6.0±0.5; GLMN-RBX1-CUL1^{CTD}~NEDD8 Rg=42.5.0±0.5, and GLMN-RBX1-CUL1 Rg=58.5±0.5; GLMN-RBX1-CUL1~NEDD8 Rg= 57.1±1.3.

C. Comparison of the theoretical SAXS profiles for the single conformers model with the MES selected two-conformer models. For better visualization the fits are shown as a I(q) experimental / I(q) model.

D. Pair distribution functions (P(r)) for for GLMN bound to RBX1 and complexes with unneddylated and neddylated “split ‘n coexpress” full-length CUL1 and CUL1^{CTD}.

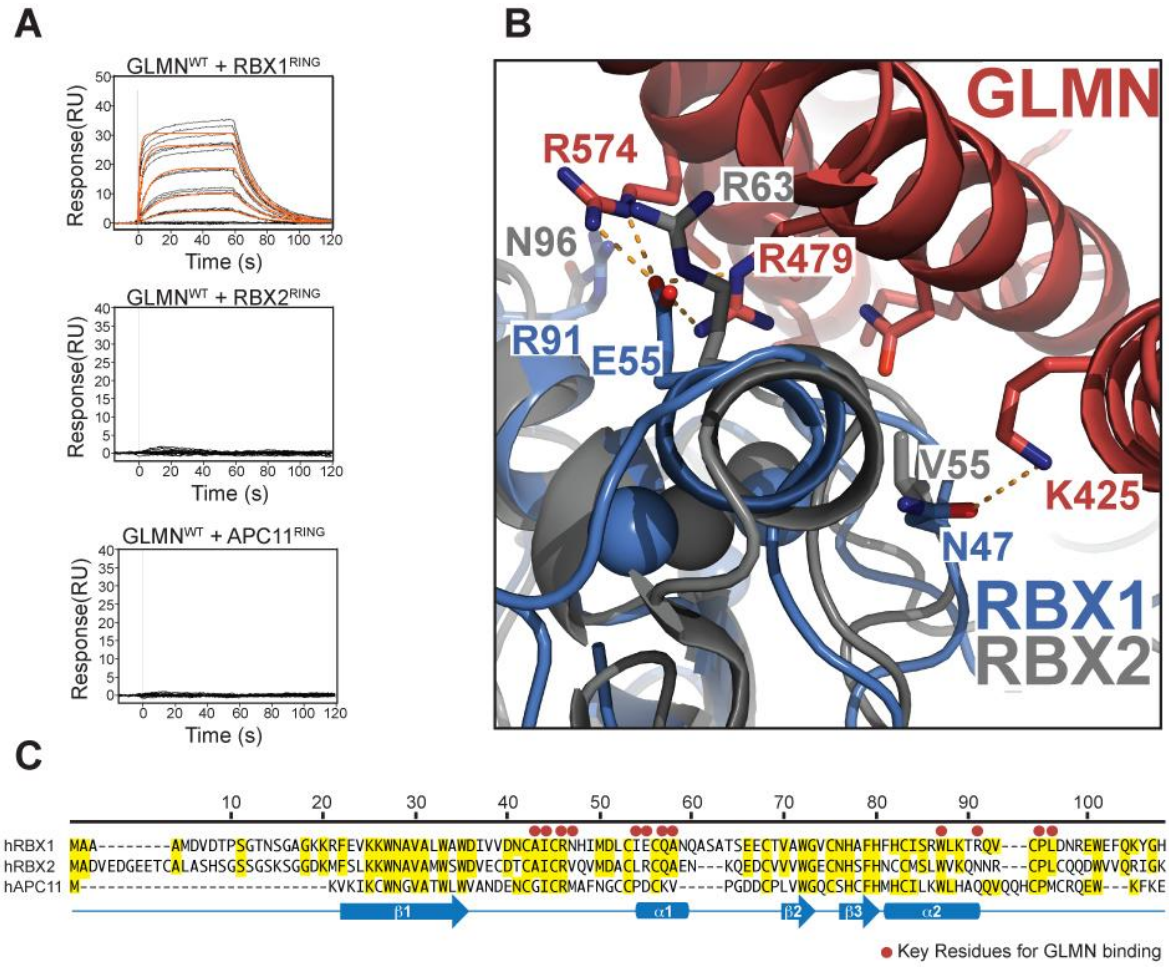

Figure S5. Structural basis for GLMN's binding specificity for RBX1 over other related RING domains

A. Representative sensorgrams from Surface Plasmon Resonance interaction assays, performed using Biacore for GLMN and RBX1^{RING}, RBX2^{RING}, or APC11^{RING}.

B. Close-up view of GLMN (red) – RBX1 (blue) interface from crystal structure, with RBX2 RING domain (grey, 2ECL.pdb) superimposed on RBX1. Key GLMN contact residues in RBX1 that differ in RBX2 are shown as sticks, with oxygens in red and nitrogens in blue. Zinc atoms are shown as spheres.

C. Alignment of human RBX1, RBX2, and APC11 sequences, with key residues mediating binding to GLMN indicated with red dots. For RBX1, residue numbers are denoted above, and secondary structures are denoted below.

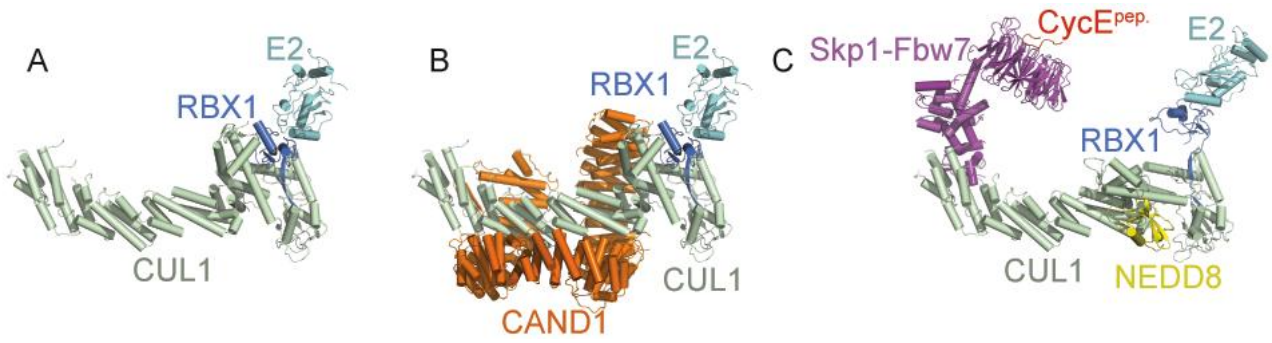

Figure S6. Structural models of SCF assemblies with E2

Structural models of (A) E2-RBX1-CUL1, (B) E2-RBX1-CUL1-CAND1, and (C) E2-RBX1-NEDD8~CUL1-SKP1-FBW7-CyclinE^{phosphopeptide} based on superimposing UbcH7-cCBL (RING) (Zheng et al., 2000) on the RBX1 RING domain of the prior RBX1-CUL1 (Zheng et al., 2002) and RBX1-CUL1-CAND1 (Goldenberg et al., 2004) structures, and on the structural model of RBX1-CUL1~NEDD8 (Duda et al., 2008) also modeled with SKP1-FBW7- CyclinE^{phosphopeptide} docked onto the N-terminal domain of CUL1 (Hao et al., 2007). The models are shown in the same orientation as Fig. 2H.

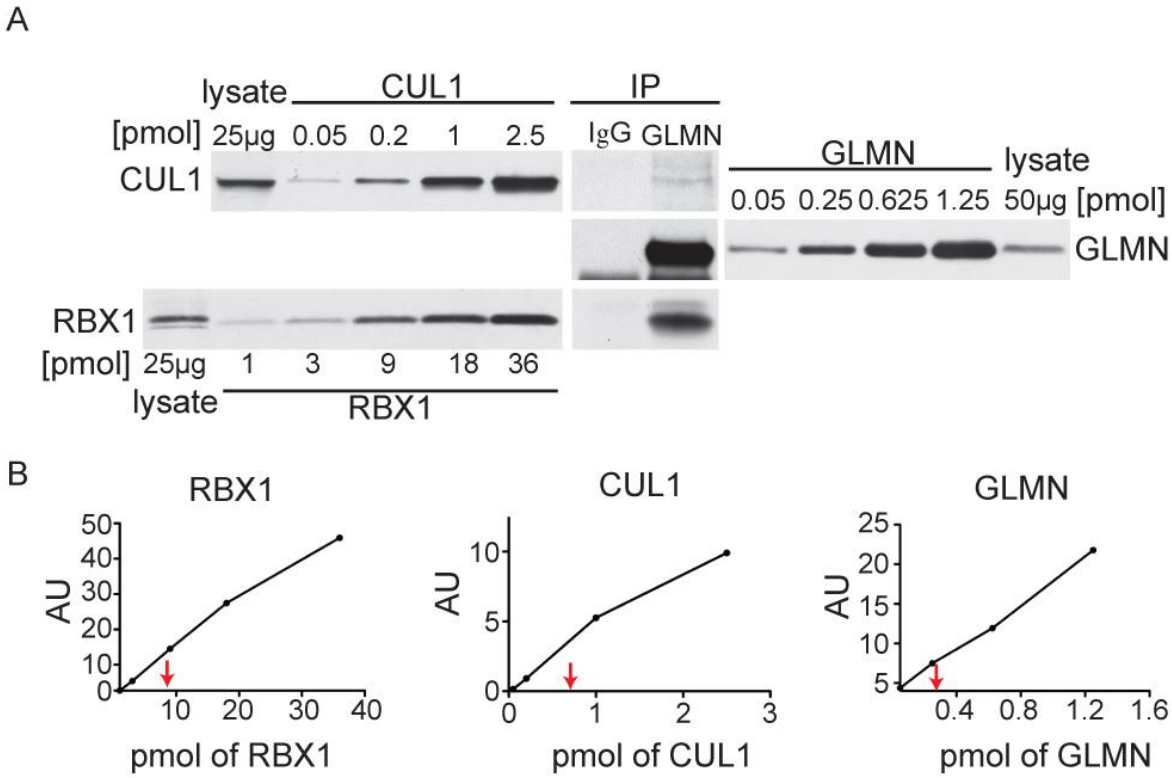

Figure S7. GLMN binds a fraction of cellular RBX1 and CUL1

A. Anti-CUL1 (top left), anti-RBX1 (bottom left), and anti-GLMN (right) western blots of the indicated amount of lysate from U2OS cells, of immunoprecipitations with IgG control or anti-GLMN antibody, loaded side-by-side with standards of known, increasing amounts of purified proteins for quantitative comparison.

B. Bands from blots above were quantified using a Syngene imaging system to generate calibration curves from the CUL1, RBX1, and GLMN standards, which were then compared with intensities of bands from lysates (red arrows) to measure 0.005 femtomoles of CUL1, 0.001 femtomoles of GLMN, and 0.077 femtomoles of RBX1 per cell.

SUPPLEMENTAL REFERENCES

Adams, P.D., Afonine, P.V., Bunkoczi, G., Chen, V.B., Davis, I.W., Echols, N., Headd, J.J., Hung, L.W., Kapral, G.J., Grosse-Kunstleve, R.W.*, et al.* (2010). PHENIX: a comprehensive Python-based system for macromolecular structure solution. Acta crystallographica *66*, 213-221.

Antos, J.M., Chew, G.L., Guimaraes, C.P., Yoder, N.C., Grotenbreg, G.M., Popp, M.W., and Ploegh, H.L. (2009). Site-specific N- and C-terminal labeling of a single polypeptide using sortases of different specificity. Journal of the American Chemical Society *131*, 10800-10801.

Arai, T., Kasper, J.S., Skaar, J.R., Ali, S.H., Takahashi, C., and DeCaprio, J.A. (2003). Targeted disruption of p185/Cul7 gene results in abnormal vascular morphogenesis. Proceedings of the National Academy of Sciences of the United States of America *100*, 9855-9860.

Brünger, A.T., Adams, P.D., Clore, G.M., DeLano, W.L., Gros, P., Grosse-Kunstleve, R.W., Jiang, J.S., Kuszewski, J., Nilges, M., Pannu, N.S.*, et al.* (1998). Crystallography & NMR system: A new software suite for macromolecular structure determination. Acta crystallographica *54*, 905-921.

Calabrese, M.F., Scott, D.C., Duda, D.M., Grace, C.R., Kurinov, I., Kriwacki, R.W., and Schulman, B.A. (2011). A RING E3-substrate complex poised for ubiquitin-like protein transfer: structural insights into cullin-RING ligases. Nature structural & molecular biology *18*, 947-949.

Delaglio, F., Grzesiek, S., Vuister, G.W., Zhu, G., Pfeifer, J., and Bax, A. (1995). NMRPipe: a multidimensional spectral processing system based on UNIX pipes. J Biomol NMR *6*, 277-293.

Duda, D.M., Borg, L.A., Scott, D.C., Hunt, H.W., Hammel, M., and Schulman, B.A. (2008). Structural insights into NEDD8 activation of cullin-RING ligases: conformational control of conjugation. Cell *134*, 995-1006.

Emsley, P., and Cowtan, K. (2004). Coot: model-building tools for molecular graphics. Acta crystallographica *60*, 2126-2132.

Goddard, T.D., and Kneller, D.G. Sparky 3 (University of California, San Francisco).

Goldenberg, S.J., Cascio, T.C., Shumway, S.D., Garbutt, K.C., Liu, J., Xiong, Y., and Zheng, N. (2004). Structure of the Cand1-Cul1-Roc1 complex reveals regulatory mechanisms for the assembly of the multisubunit cullin-dependent ubiquitin ligases. Cell *119*, 517-528.

Hao, B., Oehlmann, S., Sowa, M.E., Harper, J.W., and Pavletich, N.P. (2007). Structure of a Fbw7-Skp1-cyclin E complex: multisite-phosphorylated substrate recognition by SCF ubiquitin ligases. Molecular cell *26*, 131-143.

Hao, B., Zheng, N., Schulman, B.A., Wu, G., Miller, J.J., Pagano, M., and Pavletich, N.P. (2005). Structural basis of the Cks1-dependent recognition of p27(Kip1) by the SCF(Skp2) ubiquitin ligase. Molecular cell *20*, 9-19.

Huang, D.T., Ayrault, O., Hunt, H.W., Taherbhoy, A.M., Duda, D.M., Scott, D.C., Borg, L.A., Neale, G., Murray, P.J., Roussel, M.F.*, et al.* (2009). E2-RING expansion of the NEDD8 cascade confers specificity to cullin modification. Molecular cell *33*, 483-495.

Huang, D.T., Miller, D.W., Mathew, R., Cassell, R., Holton, J.M., Roussel, M.F., and Schulman, B.A. (2004). A unique E1-E2 interaction required for optimal conjugation of the ubiquitin-like protein NEDD8. Nature structural & molecular biology *11*, 927-935.

Huang, D.T., Zhuang, M., Ayrault, O., and Schulman, B.A. (2008). Identification of conjugation specificity determinants unmasks vestigial preference for ubiquitin within the NEDD8 E2. Nature structural & molecular biology *15*, 280-287.

Hura, G.L., Menon, A.L., Hammel, M., Rambo, R.P., Poole, F.L., 2nd, Tsutakawa, S.E., Jenney, F.E., Jr., Classen, S., Frankel, K.A., Hopkins, R.C.*, et al.* (2009). Robust, high-throughput solution structural analyses by small angle X-ray scattering (SAXS). Nat Methods *6*, 606-612.

Jubelin, G., Taieb, F., Duda, D.M., Hsu, Y., Samba-Louaka, A., Nobe, R., Penary, M., Watrin, C., Nougayrede, J.P., Schulman, B.A.*, et al.* (2010). Pathogenic bacteria target NEDD8-conjugated cullins to hijack host-cell signaling pathways. PLoS Pathog *6*.

Kleiger, G., Saha, A., Lewis, S., Kuhlman, B., and Deshaies, R.J. (2009). Rapid E2-E3 assembly and disassembly enable processive ubiquitylation of cullin-RING ubiquitin ligase substrates. Cell *139*, 957-968.

Myszka, D.G. (1999). Improving biosensor analysis. J Mol Recognit *12*, 279-284.

Otwinowski, Z., and Minor, W. (1997). Processing of X-ray Diffraction Data Collected in Oscillation Mode. Methods in Enzymology, Macromolecular Crystallography, part A *276*, 307-326.

Papalia, G., and Myszka, D. (2010). Exploring minimal biotinylation conditions for biosensor analysis using capture chips. Analytical biochemistry *403*, 30-35.

Pelikan, M., Hura, G.L., and Hammel, M. (2009). Structure and flexibility within proteins as identified through small angle X-ray scattering. Gen Physiol Biophys *28*, 174-189.

Schneidman-Duhovny, D., Hammel, M., and Sali, A. (2010). FoXS: a web server for rapid computation and fitting of SAXS profiles. Nucleic Acids Res *38*, W540-544.

Schulman, B.A., Carrano, A.C., Jeffrey, P.D., Bowen, Z., Kinnucan, E.R., Finnin, M.S., Elledge, S.J., Harper, J.W., Pagano, M., and Pavletich, N.P. (2000). Insights into SCF ubiquitin ligases from the structure of the Skp1-Skp2 complex. Nature *408*, 381-386.

Siergiejuk, E., Scott, D.C., Schulman, B.A., Hofmann, K., Kurz, T., and Peter, M. (2009). Cullin neddylation and substrate-adaptors counteract SCF inhibition by the CAND1-like protein Lag2 in Saccharomyces cerevisiae. The EMBO journal *28*, 3845-3856.

Spirig, T., Weiner, E.M., and Clubb, R.T. (2011). Sortase enzymes in Gram-positive bacteria. Molecular microbiology *82*, 1044-1059.

Spratt, D.E., Wu, K., Kovacev, J., Pan, Z.Q., and Shaw, G.S. (2012). Selective recruitment of an E2~ubiquitin complex by an E3 ubiquitin ligase. The Journal of biological chemistry in press. doi: 10.1074/jbc.M112.353748.

Svergun, D.I. (1992). Determination of the regularization parameter in indirect-transform methods using perceptual criteria. J Appl Cryst *25*, 495-503.

Svergun, D.I., Petoukhov, M.V., and Koch, M.H. (2001). Determination of domain structure of proteins from X-ray solution scattering. Biophysical journal *80*, 2946-2953.

Tron, A.E., Arai, T., Duda, D.M., Kuwabara, H., Olszewski, J.L., Fujiwara, Y., Bahamon, B.N., Signoretti, S., Schulman, B.A., and DeCaprio, J.A. (2012). The Glomuvenous Malformation Protein Glomulin Binds Rbx1 and Regulates Cullin RING Ligase-Mediated Turnover of Fbw7. Molecular cell *46*, 67-78.

Vlach, J., Hennecke, S., and Amati, B. (1997). Phosphorylation-dependent degradation of the cyclin-dependent kinase inhibitor p27. The EMBO journal *16*, 5334-5344.

Walden, H., Podgorski, M.S., Huang, D.T., Miller, D.W., Howard, R.J., Minor, D.L., Jr., Holton, J.M., and Schulman, B.A. (2003). The structure of the APPBP1-UBA3-NEDD8-ATP complex reveals the basis for selective ubiquitin-like protein activation by an E1. Molecular cell *12*, 1427-1437.

Zheng, N., Schulman, B.A., Song, L., Miller, J.J., Jeffrey, P.D., Wang, P., Chu, C., Koepp, D.M., Elledge, S.J., Pagano, M.*, et al.* (2002). Structure of the Cul1-Rbx1-Skp1-F boxSkp2 SCF ubiquitin ligase complex. Nature *416*, 703-709.

Zheng, N., Wang, P., Jeffrey, P.D., and Pavletich, N.P. (2000). Structure of a c-Cbl-UbcH7 complex: RING domain function in ubiquitin-protein ligases. Cell *102*, 533-539.